Reducing Multi-Separation Color Moiré by a Variable Undercolor Removal and Gray Component Replacement Strategy

Raja Balasubramanian▲ and Reiner Eschbach✦

Xerox Digital Imaging Technology Center, Webster, New York

One common artifact in color printing is the moiré caused by the superposition of the different color separations. This problem is well known and a common approach to minimize the moiré is the use of rotated halftone dots of precise frequency and angle for the different separations. In low resolution devices, the precise relationship between the different separations is commonly hard to satisfy and compromises have to be made. This paper describes a method to vary the undercolor removal (UCR) and gray component replacement (GCR) schemes employed as a function of the predicted inter-separation moiré in order to allow for a better trade-off in the halftone design.

Journal of Imaging Science and Technology 45: 152–160 (2001)

Introduction

Printing a color image on paper requires that the desired digital color values of the input image are transformed to a reflectance pattern of an ink layer on paper. In most cases, the ink layer is bi-level in nature, which means that no pointwise modulation of the ink density can be achieved by the process. Some processes, like Dye Diffusion Thermal Transfer (D2T2), allow this local modulation, but for the purpose of this article, we will restrict ourselves to binary (or other low number of output density levels) printing devices such as xerography, ink-jet, etc.

In all devices that are not capable of actually rendering the continuous data directly onto paper, an intermediate halftoning step has to be performed. The best known halftoning process is the conventional rotated dot halftoning as it is found in every magazine or newspaper photo. Other halftoning methods include stochastic halftoning, adaptive halftoning, or even iterative halftoning schemes. For the purpose of this article, we will group the different halftoning methods into periodic halftoning methods and non-periodic halftoning methods, where we consider a method to be periodic if it exhibits a strong frequency component in its Fourier spectrum. The most common of the periodic halftoning methods, again, is the rotated dot halftoning[1,2] but other methods include ARIES,[3] threshold modulated error diffusion[4] and dot-to-dot diffusion.[5,6] Good collections of digital halftoning work can be found in Refs. 7, 8, and 9.

Original manuscript received June 22, 2000

✦ IS&T Fellow

▲ IS&T Member

Color Plates 12 and 13 are printed in the color plate section of this issue, p. 173.

Due to some inherent advantages, rotated dot screens are the most common halftoning method. The color reproduction of rotated dot schemes is more robust with respect to mis-registration errors than color reproduction using other halftoning schemes (e.g., dot-on-dot or dot-off-dot). In order to achieve good overall print quality, however, the angles between the different color separations have to be precisely controlled, or moiré will occur. This precise control of the screen angles is generally not possible in digital systems with their inherent discrete resolution. At the high resolutions commonly used in offset printing (e.g., $\geq 2400 \times 2400$dpi), the discrete nature of the screen is normally not a critical issue. The problem persists, however, at resolutions commonly found in xerographic printers.

Because moiré is a strong function of the relative screen angles, especially of the *c,m,k* separations, many approaches have been explored for mitigating moiré patterns via halftone screen and screen angle design. However, as will be shown in this paper, moiré is also a strong function of the geometry of the individual halftone dot, specifically the dot area coverage of the halftone dot. It is this dependence that is described and exploited in this paper. More specifically, a method is described that reduces the *c,m,k* moiré by using a variable undercolor removal (UCR) and gray component replacement (GCR) scheme for a given halftone screen. Preliminary work was published in a conference proceeding.[10] This article is a more detailed and complete description of the work.

Modeling Moiré In Color Printing

The effect of moiré in color printing has long been known and has led to the common color layout of using cyan and magenta at plus and minus 15°, black, or key, at 45° and yellow at 0°. In this scenario, cyan, magenta and black use the identical screen frequencies. In this way, the interaction, or moiré, between cyan and magenta has identical frequency and orientation as the black separation. The result is a zero frequency moiré

that is stable with respect to shifts of the individual separations, but sensitive to any errors in frequency or rotation angle. The yellow separation often uses the identical screen frequency and geometry as the other separations, but suggestions have been made to either change the frequency of the yellow screen[11] or to use a different screen geometry, e.g. hexagonal screens.[12] In general, the moiré involving the yellow component has been of minor importance compared to the moiré of the other separations.

Other approaches to avoid multi-color moiré in printing exist, such as using a non-periodic, or quasi-periodic halftone screen in one of the separations, for example in the black separation.[13]

Common Types of Moiré

There are two basic types of color moiré that influence the print quality. The first type is the 2 colorant moiré commonly found between yellow and cyan or yellow and magenta. The second, and normally more disturbing, moiré is caused by the superposition of cyan, magenta, and black. It should be noted that the moiré is caused by the unwanted absorption of the printing materials. With "perfect" inks, none of the described two or three color moiré would occur, since only the black separation would interact with the other separations. This paper will restrict itself to cover the commonly more important three colorant moiré case of the cyan, magenta and black superposition.

One interesting aspect of color moiré in printing is that it is not only a function of the spectral absorption of the colorants, but also a rather direct function of the area coverage of the dot. This dependency can be illustrated using a simple 1-dimensional (1-D) example. Assume the optical superposition of three spectral transmittance functions, $T_c(x, \lambda)$, $T_m(x, \lambda)$ and $T_k(x, \lambda)$ corresponding to the cyan, magenta, and black ink layers respectively, in a printing process. Here, x denotes the spatial location, and λ the wavelength. Let us denote the reflectance of the paper as $R_p(\lambda)$, and to further simplify the analysis, we will assume that there is no scattering within the paper and that the yellow separation can be neglected. Without any physical interaction between the separations, i.e., no ink running, etc., the overall reflectance function can be described as:

$$R(x,\lambda) = R_p(\lambda)T_c(x,\lambda)^2 T_m(x,\lambda)^2 T_k(x,\lambda)^2 = \frac{1}{R_p(\lambda)^2} R_c(x,\lambda)R_m(x,\lambda)R_k(x,\lambda) \quad (1)$$

where $R_i(x, \lambda) = R_p(\lambda)T_i(x, \lambda)^2$, $i = c, m, k$.

Calculating the Moiré Parameter

Each of the individual reflectances $R_i(x,\lambda)$ in Eq. 1 has the form of a periodic halftone dot (in the 1-D example a line screen) and can be described by its Fourier series:

$$R_i(x,\lambda) = 1-\left[\left(1-R_i(\lambda)\right)\right]\cdot\left[\frac{b_{i,0}}{2}+\sum_{n=1}^{\infty} b_{i,n}\cos\left(\frac{2\pi\, nx}{P_i}\right)\right], \quad (2)$$

where

- $R_i(l)$ is the wavelength dependent component of the reflectance of the i-th separation,
- P_i is the periodicity of the halftone screen of separation i and
- $b_{i,n}$ are the Fourier coefficients of the halftone screen, for
- $i = c,m,k$.

The Fourier coefficients for each separation are computed as:

$$b_n = \frac{4}{P}\int_0^{P/2} S(I,x)\cos\left(\frac{2\pi\, nx}{P}\right)dx\,, \quad (3)$$

where $S(I,x)$ denotes the actual reflectance distribution of the halftone dot which is a function of both spatial location and input level I. The reflectance is expressed as a Fourier series in order to facilitate the approximations that will be done in subsequent steps. Eq. 2 is a complete description of a periodic halftone screen, containing all frequency information. With the Fourier series description, the overall reflectance of Eq. 1 can be rewritten as

$$R(x,\lambda) = \frac{1}{R_P(\lambda)^2}\cdot\prod_i\left\{1-\left[1-R_i(\lambda)\right]\cdot\left[\frac{b_{i,0}}{2}+\sum_{n=1}^{\infty} b_{i,n}\cos\left(\frac{2\pi\, nx}{P_i}\right)\right]\right\} \quad (4)$$

In order to get an estimate of the moiré between different separations we will concentrate on the components of Eq. 4 that are involved in the visual moiré. Some assumptions can be made to determine the relevant frequencies.

- First, the visual moiré is caused by low frequency components, well below the normal screen frequency. This means that all terms that have a frequency equal or higher than the original screen frequencies (n=1) can be neglected.
- Secondly, the periodicities of the individual separations are comparable in magnitude, i.e., $P_i \approx P_j$. In this case, only the same frequency components ($n_i = n_j$) of the different separations are relevant.
- Thirdly, the magnitude of the Fourier coefficients generally decreases with order n (and often decreases faster than this if the dot profile is smoother than a perfect rectangle).

Under these assumptions, we can disregard every term higher than first order (n >1) in the consideration of the moiré. The result of that approximation for the reflectance of the individual separations leads to an overall reflectance of:

$$R(x,\lambda) \approx \frac{1}{R_P(\lambda)^2}\cdot\prod_i\left\{1-\left[1-R_i(\lambda)\right]\cdot\left[\frac{b_{i,0}}{2}+b_{i,1}\cos\left(\frac{2\pi\, x}{P_i}\right)\right]\right\}. \quad (5)$$

The approximate reflectance still contains the fundamental screen frequencies and thus the individual screens. Also, Eq. 5 still covers all two color moirés, including the ones involving yellow by having the index i

run over all available separations *c,m,y,k*. Of all the frequency components contained in Eq. 5, only the term covering the periodic components is involved in the color moiré:

$$R_{moiré}(x,\lambda) = \frac{1}{R_P(\lambda)^2}\cdot\prod_i\left\{\left[1-R_i(\lambda)\right]\cdot b_{i,1}\cos\left(\frac{2\pi\ x}{P_i}\right)\right\},$$

or, for the considered case of the three color *c,m,k* moiré:

$$R_{moiré}(x,\lambda) = \frac{1}{R_P(\lambda)^2}\left[1-R_c(\lambda)\right]\cdot\left[1-R_m(\lambda)\right]\cdot\left[1-R_k(\lambda)\right]\cdot b_{c,1}b_{m,1}b_{k,1}\cdot\cos\left(\frac{2\pi x}{P_c}\right)\cos\left(\frac{2\pi x}{P_m}\right)\cos\left(\frac{2\pi x}{P_k}\right) \quad (6)$$

One well known aspect is obvious from Eq. 6: if the individual reflectances have no unwanted absorptions, i.e., $[1\text{-}R_i(\lambda)][1\text{-}R_j(\lambda)] \equiv 0$, no moiré will occur. The terms in Eq. 6 can be grouped to emphasize the moiré dependency on both the spectral absorption of the ink/toner and on the Fourier coefficient of the input data as:

$$R_{moiré}(x,\lambda) = \Lambda(\lambda)\cdot M(b)\cdot\prod_i\cos\left(\frac{2\pi x}{P_i}\right). \quad (7)$$

The moiré is thus determined by three parameters, (1) the spectral characteristic, encapsulated in $\Lambda(\lambda)$, (2) the frequency characteristic encapsulated in the product of cosines, and (3) one additional term, *M(b)* that depends on the Fourier coefficients of the periodic halftone pattern. All three terms influence the resultant moiré, whereby the first two terms influence the amplitude of the moiré and the third term influences its frequency.

The first term, $\Lambda(\lambda)$ encapsulates the spectral characteristic of the colorants and will be considered predetermined for the purpose of this article. The third term, the product of cosines, reflects the common design choices in rotated dot halftoning, and it is this term that is normally minimized in order to obtain a moiré free reproduction. For the purpose of this article, we will assume that standard processes have been used to minimize this term, but that the remaining moiré is still objectionable. In this case, only the second term is left as a potential for modification.

The second term, *M(b)*, is a function of the first order Fourier coefficient of the series expansion of the halftone dot. Since the actual shape of the halftone dot is a function of the digital input level of the corresponding separations, the Fourier coefficients $b_{i,1}$ are in effect functions of the input level:

$$M(b) = b_{c,1}(I_c)\cdot b_{m,1}(I_m)\cdot b_{k,1}(I_k).$$

In order to better understand the relationship between the moiré parameter *M* and the input data, it useful to derive the functional dependence between *M* and the input data *I*. Here, we make use of the fact that the Fourier series of Eq. 2 was normalized between 0 and 1 by factoring out the individual reflectance components. This in turn means that the input intensity is also normalized to $0 \le I \le 1$, i.e., between no area coverage and full area coverage. Figure 1 shows the geometry of the binary 1-dimensional halftone dot on paper. From this, we can derive the Fourier series coefficients of Eq. 2. The Fourier coefficients for $n > 0$ can be written as

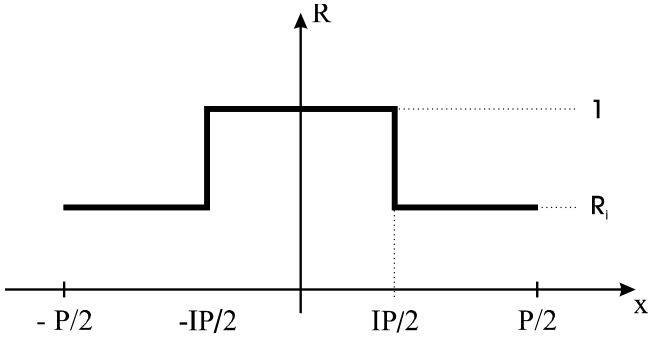

Figure 1. 1-D spatial reflectance profile of binary dot.

$$b_{i,n} = \frac{4}{P_i}\int_0^{P_i/2} S_i(I_i,x)\cdot\cos\left(\frac{2n\pi\ x}{P_i}\right)dx = \frac{4}{P_i}\int_0^{I_iP_i/2}\cos\left(\frac{2n\pi\ x}{P_i}\right)dx = \frac{2}{n\pi}\sin(n\pi\ I_i) \quad (8)$$

Equation 8 shows the dependency of the Fourier coefficient $b_{i,n}$ on the input data *I,* and consequently, via Eq. 7, the dependency of the moiré on the input data. Eq. 8 also verifies the ingoing assumption that the Fourier coefficients generally decrease with increasing order *n*.

The moiré parameter *M* is thus given by

$$M(b) = \frac{8}{\pi^3}\sin(\pi\ I_c)\sin(\pi\ I_m)\sin(\pi\ I_k). \quad (9)$$

It is easily shown that *M* is maximized for $I_i = 1/2$.

Equations 8 and 9 were derived for an idealized binary halftone, but the generalization to a more complicated halftone profile can simply be obtained by inserting a more complex halftone dot shape function *S(I,x)* into Eq. 8.

The moiré parameter *M* gives an indication of the moiré amplitude in the halftone superposition in cases where the other parameters are fixed. It is important to remember, that the value of the parameter does not give an indication of the total strength of the moiré, since halftone frequencies, angles and colorants also influence the total moiré as indicated in Eq. 7.

Creating a 2-D Approximation From the 1-D Model

The above description for the moiré parameter was derived using a 1-dimensional model. This model is directly applicable to line screen scenarios, as they are common in a large set of current color laser printers/copiers, but the extension to a 2-dimensional rotated dot model has to be examined. Figure 2 shows a typical halftone dot at 45° angle for different input levels. As can be seen from Fig. 2, the resultant halftone has—with respect to opening ratio—a strong resemblance to a line screen for an input level $I = 1/2$. Cutting the half-

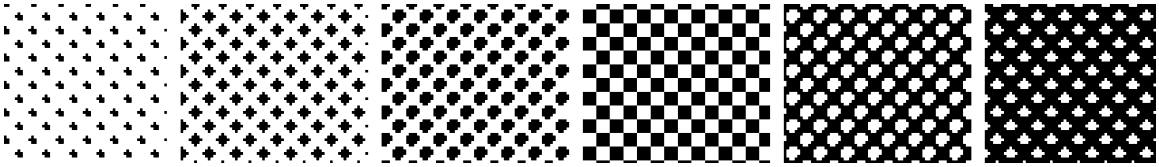

Figure 2. Halftone dot structure for the *K* separation for digital inputs (top to bottom): 32, 64, 96, 128, 160, 192.

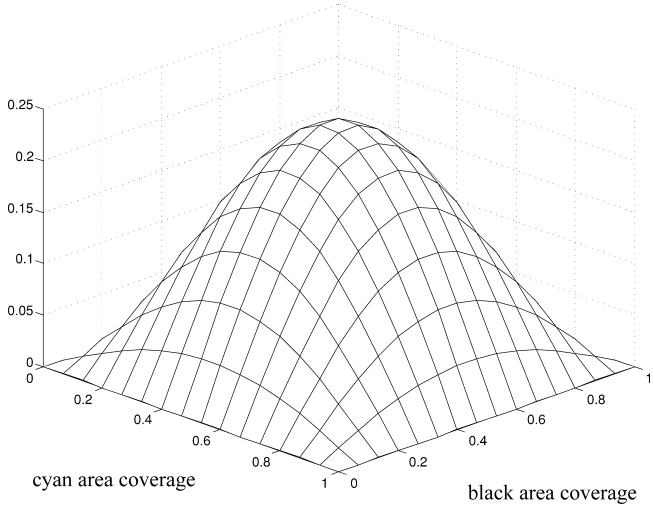

Figure 3. Theoretical moiré amplitude as a function of I_c and I_k area coverages (I_m = 0.63).

tone along vertical or horizontal lines gives an opening ratio of 50% at exactly the same input level of I = 1/2. As first order approximation, we will thus assume that the 1-dimensional description can directly be applied to 2 dimensions. It should be noted that this is a rough approximation, the validity of which has to be experimentally tested.

Under the assumption given above, a 3-D plot of the parameter I_M as a function of I_k and I_c can be created. Figure 3 shows this plot for a constant magenta area coverage of 63% (I_m = 0.63). As can be seen from Fig. 3, the parameter M goes to zero at the boundary, i.e., whenever one of the input values is 0 or 1, and has its maximum at $I_c = I_k$ = 1/2. The location of the maximum in Fig. 3 does not change if the input value for magenta is changed from 40% to any other value. The absolute maximum of the function is reached for $I_c = I_k = I_m$ = 1/2, resulting in M = 0.258.

Three and Four Component Color Descriptions

The derivation of the moiré parameter M helped in understanding the relationship between input data and output moiré strength. With the help of the parameter M, it is possible to predict the moiré amplitude of the specified halftone superposition for a given input I_c, I_m, and I_k. An interesting application of the moiré parameter would be the inverse problem, namely: given a moiré parameter M, can we find a different I_c, I_m, I_y, I_k. combination that yields the identical output color with a lower moiré parameter?

If I_c, I_m, I_y, and I_k are independent variables, no changes can be made, and the moiré is intrinsically linked to the four components. However, in the area of color printing, the visual color representation of the input data is determined by a three component vector. This three component vector can described in the four colorant system in an underdetermined way. This means that there will be a potentially large number of possible four colorant combinations that are equivalent to a given three component input, yielding the same visual appearance. In different words, a large number of *c, m, y, k* quadruplets can be used to render a single r,g,b, or Lab triplet. The input function I_k for the k-separation is not an independent variable, but actually a function of the inputs for the c, m, and y-separation, $I_k = f(c, m, y)$. Consequently, the moiré parameter can be used in determining which *c, m, y, k* quadruplet would yield the correct color with a minimum likelihood of moiré.

Effect of the UCR / GCR on Moiré

In the previous section, we briefly discussed the underdetermined nature of a four color printing system with respect to the three color input data. This section will take a closer look at three-to-four mapping and some of the underlying motivations in designing a UCR/GCR strategy. This will then enable us to use the moiré parameter to select a colorant quadruplet that fulfills boundary conditions with respect to moiré.

Undercolor removal (UCR) and gray component replacement (GCR) are techniques for transforming a *c,m,y* combination to a *c,m,y,k* combination via suitable addition of *k* and possible reduction of *c,m,y*. UCR and GCR algorithms are designed to achieve the best tradeoff among several factors, the key ones being the ink area coverage, the response along the neutral axis, the overall color gamut, and the smoothness of sweeps from neutral to highly chromatic colors.

In this way, the UCR/GCR strategy creates a unique mapping of the input triplet to the output quadruplet by introducing additional requirements into the system. The UCR/GCR commonly does not include provisions for incorporating inter-separation moiré effects, but it can be understood from Eq. 9 that the UCR/GCR will directly influence the moiré strength by modifying the functional dependence of I_k on I_c, I_m, and I_y. Equation 9 gives us a simple method to take the moiré magnitude as an additional factor into account for the UCR/GCR. It is easily seen that Eq. 9 is strongly influenced by the relative amounts of *c, m*, and *k*, which are intimately related to the UCR/GCR strategy. Here, one has to remember that the *k*-component - and consequently $b_{k,n}$— has been generated by a color correction algorithm and that several (*c, m, y, k*) quadruplets would result in the identical color. One way to eliminate the three component moiré is to eliminate *k*, thereby setting $b_{k,n}$ to zero, and thus M to zero in Eq. 9. This is a trivial solution and equivalent to a standard three color process. This trivial solution will be ignored since it would eliminate the advantages from the use of *k*, e.g., larger gamut in the dark regions of color space.

The only solutions that give a moiré parameter identical to zero are the ones where at least one of the separations *c, m,* or *k* is either full "on", or full "off". In real

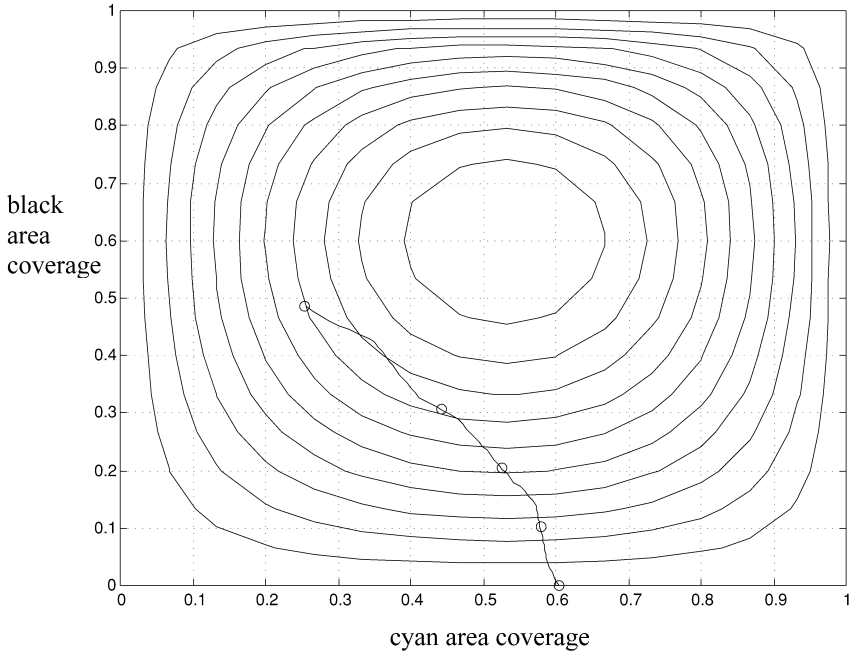

Figure 4. Plot of I_c versus I_k yielding same LAB value superimposed on contour plot of moiré amplitude. 5 points marked by circles are used for experimental verification.

situations, however, a zero moiré amplitude is not necessary. It is sufficient to have the moiré amplitude below a certain limit so that the moiré is no longer visible to the user. An estimate of the moiré visibility can be made from the moiré parameter M described in Eq. 9. It should be understood that the parameter M reflects the strength of the moiré, but that the moiré visibility is also influenced by other factors such as frequency and bias. In the following, we will neglect the other factors, since, for example, the moiré frequency can not be influenced by the UCR/GCR strategy.

Incorporating the Moiré Parameter *M* into the GCR/UCR

Typical GCR/UCR strategies are a function of the minimum component of the requested color. Commonly this means that GCR/UCR is performed for darker colors, but the UCR is set to zero for light colors and colors with high chroma. This article proposes to augment that strategy and to use a UCR/GCR that is also a function of the actual color (and not only the minimum component) of the input pixel. This would mean that the UCR/GCR in the red area of color space could be different from the UCR/GCR used in the blue area for the same minimum c,m,y value, since a moiré is more likely to be encountered in the blue area ($I_c \approx I_m$) than in the red ($I_c \ll I_m$). Forcing the same UCR/GCR strategy on the entire color space, as is commonly done, negatively impacts the potential print quality in some parts of the color gamut, e.g.: the red sections of an image would be sub-optimally represented, if visible moiré in the blue was used to alter the global UCR/GCR design.

As mentioned above, examination of Eq. 9 suggests that the UCR/GCR in the red area of color space should be different from the UCR/GCR used in the blue area for the same minimum c,m,y value. Equation 9 can be used to restrict the GCR/UCR scheme in the blue area (c and m are present) to those schemes that have a small moiré value. In the red area, the c, m, k-moiré limitation disappears. GCR/UCR schemes that do not take this into account run the risk of introducing a moiré in one area or of using a sub-optimal GCR/UCR in another area of color space.

Figure 4 is a contour plot version of the moiré model of Fig. 3. Also shown on this plot is a locus of several c,m,y,k combinations that map to the same output CIELAB color for a Xerox 5790 laser printer. In order to obtain this locus, one c,m,y,k quadruplet was chosen in the purple region of color space (as this is the most problematic region in terms of 3 colorant moiré, and is hence of most interest for this analysis). The corresponding colorimetric value (in our case CIELAB) was computed with the use of a printer model. The printer model was a spectral cellular Neugebauer model[14] derived to predict CIELAB color for a given input cmyk and given halftone screens used with the 5790. Using this printer model, a search was performed to obtain other c,m,y,k quadruplets whose output CIELAB color was within one ΔE^* of the color of the original quadruplet. (Throughout the article, "ΔE^*" refers to the 1976 ΔE^*ab metric.) The search resulted in 64 c,m,y,k quadruplets. The moiré parameter was calculated for all these quadruplets using Eq. 9. Out of the 64 quadruplets, a smaller sample set of five points, indicated as circles in Fig. 4, was chosen for further experimental verification.

Note that the equi-CIELAB locus represents a family of UCR/GCR strategies, with increasing use of the k separation from the lower right to the upper left portion of the curve. Observe also that the locus cuts through different contours of the moiré plot, with the minimum (i.e., zero) moiré occurring at the $k = 0$ (lower right) endpoint.

Modification of UCR/GCR Schemes

The analysis just described can be used to optimize the UCR/GCR strategy to minimize or constrain the

moiré amplitude. Several approaches for doing this are now discussed.

Minimum Moiré Solution

The preceding analysis can be used to find the minimum moiré solution for each *cmyk* quadruplet of interest. We begin with the standard color correction process, i.e., we assume a mapping from a set of input CIELAB values (e.g., values in a 3-dimensional lookup table) to a set of *cmyk* quadruplets derived according to a standard UCR/GCR approach. For each such *cmyk* quadruplet, the searching process described previously is performed, and an alternative quadruplet is derived which yields the same CIELAB color (within a given tolerance), but with minimum moiré. Such an extensive search-based method presents a considerable computational effort, but one has to keep in mind that the computation is done once in the creation of the color correction tables and that it does not influence the performance of the overall printing system. The advantage of the search-based method is that a minimum moiré amplitude can be determined and the corresponding *c,m,y,k* quadruplets can be used in printing.

For most applications, an extensive search is not necessary, and a limited search would be sufficient. In order to restrict the actual search space for the algorithm, several other types of moiré reduction schemes can be used.

Moiré Amplitude Restriction

The search-based approach to moiré reduction was able to determine an "optimal" *c,m,y,k* quadruplet with respect to the described moiré parameter. At the same time, the computed quadruplet might have a considerable deviation in its individual components from the initial quadruplet determined by the conventional UCR/GCR strategy. Assuming that the original strategy was chosen for some specific merit in connection with, e.g., the actual output device, this strong deviation might not be desired. An alternative scheme would be to apply an adjustment only to those *c,m,y,k* values for which the moiré amplitude M exceeds a preset limit, rather than finding the lowest possible moiré parameter.

A simple scheme can be used for the adjustment: the input component with the largest amplitude is examined and changed (this is done by decreasing area coverage for $I < 0.5$ and increasing area coverage for $I \geq 0.5$) and the change is monitored. The remaining components may be adjusted to compensate for this change, using the printer model. This approach is a limited search-based approach that severely limits the actual search space when compared to the full minimization attempt described earlier. Again, the approach might take several computations per point in color space, but it is only performed once on a selected number of points during the generation of the color profile. Note that a set of tone reproduction curves (TRCs) often follow the UCR/GCR module in the image path. In this case, these TRCs must be incorporated into the moiré model.

Input Area Coverage Restriction

Another possible scheme even further reduces the search space for the *c,m,y,k* quadruplet. In this scheme, the area coverage of just one of the color components is considered. In a straightforward implementation, the black component (*k*) is considered to trigger the quadruplet modification. Because the model (6) predicts the highest moiré around 1/2 area coverage, the chosen component could be restricted to $I < 1/2 - \delta$ and $I > 1/2 + \delta$ for the "blue" part of color space, where "blue" can be defined by an approximation to hue, derived from the input *c,m,y,k*. The exact bounds of the "blue" part of the color space are unimportant in the scheme and a simple approximation from the input *c,m,y,k* quadruplet is sufficient. The modification of one of the components again will be compensated for by changing the values of the remaining three components using the printer model.

Blending of UCR/GCR Schemes

Another scheme uses the moiré parameter M to select between different conventional UCR/GCR schemes. In this scheme, the actual search is limited to the few *c,m,y,k* quadruplets that were determined a priori from a selected number of UCR/GCR schemes. In this case, the "preferred" UCR/GCR scheme is used as the initial scheme. If the moiré parameter is above a set threshold, the other schemes are evaluated at that point in color space and one of the other schemes is selected. This selection might be done by picking the scheme with the lowest moiré parameter, but it might alternatively be done by picking the scheme that creates the most similar c,m,y,k quadruplet to the preferred scheme without exceeding the preset moiré parameter threshold.

The final GCR/UCR scheme then uses the original scheme, adapted to the moiré scheme in a limited hue range of color space. Smooth transitions are achieved by conventional blending techniques.

Experimental Results

In the previous sections, several assumptions and predictions have been made. This section will describe the experiments performed in order to verify the model and model predictions.

Experimental Verification of the 2-D Moiré Model

In order to verify the model formulated in the second section, an experiment for the visual estimation of the moiré was performed. For this experiment, color prints were generated for I_c, I_m, and I_k combinations, intentionally using a halftone screen set that was found to exhibit moiré due to a slight frequency mismatch, as expressed by the product of cosines in Eq. 7.

The halftone patches were created and printed for observer evaluation. The patches were printed at large magnification in order to minimize printer influences and printability issues, such as mechanical and optical dot gain. The large format prints were posted on a wall and the observers were asked to identify the patches with the strongest moiré from a distance. The same viewing distance was used for all observers. The angular moiré frequency used in the visual test differed from the frequency that would have been obtained when examining a full resolution print at normal viewing distance, however, the absolute moiré frequency does not influence the relative moiré amplitudes (the frequency does not change as a function of area coverage).

Taking an average of the 9 observer responses, the maximum moiré was found to occur at $I_c = 0.53$, $I_k = 0.6$, and $I_m = 0.63$ (i.e., area coverage levels that are slightly higher than that predicted by the model). The standard deviation of the observer responses was 0.09, indicating considerable uncertainty expressed by some of the observers. This uncertainty is in perfect agreement with the broad maximum predicted by the moiré function shown in Fig. 3.

The experimentally obtained data can be used to adjust the moiré parameter by aligning the location of maximum in the observer response with the location of

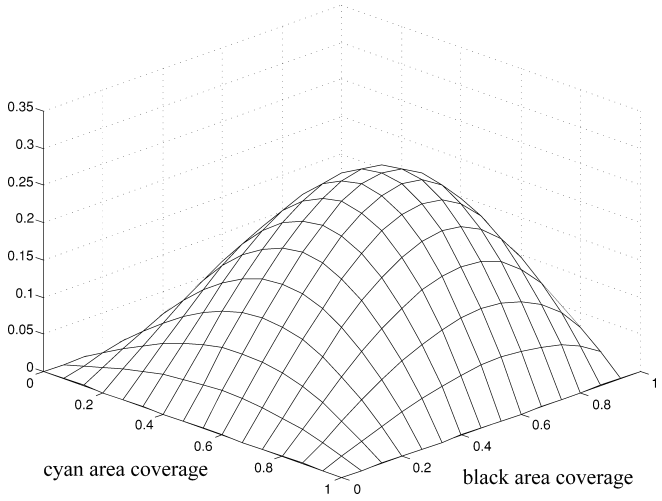

Figure 5. Visually corrected moiré amplitude as a function of I_c and I_k area coverages (I_m = 0.63).

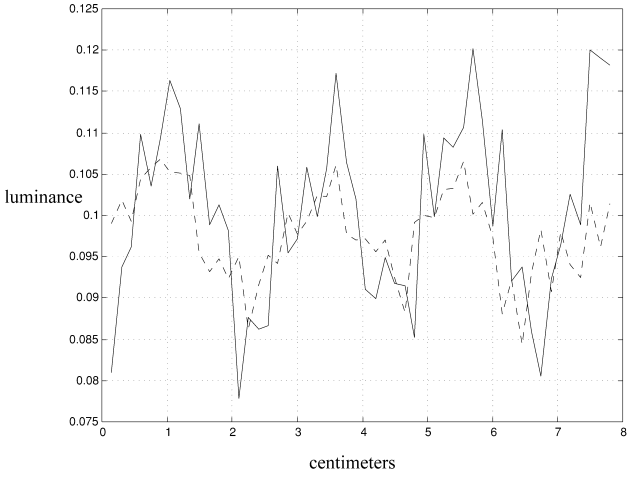

Figure 6. Luminance profiles of second (dashed) and fourth (solid) patch from Plate aa.

TABLE I. Comparison of the Predicted Moiré Parameter With the Rank-Ordered Data from Ten Observers.

Patch	c,m,y,k area coverages	Model parameter M	Scaled Model Parameter (1 to 4.3)	Observer Ranking		
				Average	Minimum	Maximum
1	0.60 0.54 0.28 0.	0	1	1	1	1
2	0.58 0.51 0.25 0.10	0.08	2.3	2.2	2	4
3	0.53 0.47 0.21 0.20	0.15	3.5	4.1	3	5
4	0.44 0.40 0.16 0.31	0.20	4.3	4.3	3	5
5	0.25 0.27 0.01 0.49	0.14	3.3	3.4	2	5

the maximum in the model. The adjustment was performed by applying a power law to I_c, I_m and I_k in Eq. 9 so that the maxima of the model and the visual experiment coincided. Figure 5 shows the modified model using the observer data and by comparing Fig. 5 with Fig. 3, one sees that the observer adjustment only has a small effect on the model. It should be noted that the adjusted moiré parameter was used in the contour plot of Fig. 4.

In order to gather data on moiré detectability thresholds, in the same visual experiment, the nine observers were also asked to select one patch for which the moiré was just barely detectable. The theoretical moiré M was then computed for each of the nine chosen patches. The average, minimum, and maximum values of M from this analysis were 0.053, 0.02, and 0.091 respectively. This information will be used in a following section to adjust the UCR/GCR so that the moiré falls below the detectable threshold.

Experimental Verification of the Model Prediction. If the model is a good description of the actual three color moiré, a strong correlation should exist between the visible moiré of the different c,m,y,k patches and the calculated moiré parameters in Fig. 4. This correlation was tested in two experiments, one based on observer response and one based on colorimetric measurement.

Visual Verification of the Moiré Parameter. In order to visually evaluate the correlation between moiré parameter and visible moiré, the five c,m,y,k combinations indicated in Fig. 4 were printed. The patches are reproduced in **Color Plate 12 (p. 173)** with I_k increasing from left to right. From **Color Plate 12** we can see that a good correlation exists between the moiré parameter M and the visual impression of the existing moiré. Please note that since the patches were originally derived for rendering to the Xerox 5790 printer, the offset printing process for this journal likely will have impacted the color reproduction as well as the visibility of moiré. For verification, the five patches, printed on the 5790, were also evaluated by ten observers in an office setting without control of illumination or viewing distance. The observers rank-ordered the patches with respect to the strength of the visibility of the moiré. A high ranking corresponded to high moiré visibility. This experiment was performed as a "quick" verification of the model. The result of the observer rankings is given in Table I. When the model predictions are scaled to the range of the average of observer rankings, a good agreement is achieved between average observer ranking and model prediction.

Colorimetric Verification of the Moiré Parameter. Another important aspect is the correlation between the moiré parameter and the measured variations in the patches. For this purpose, the patches were printed under slight integer magnification and measured using an automated measurement station. The moiré periodicity of the prints was approx. 19.5 mm. The automated measurement station took one measurement every 1.5 mm over approximately 8 cm, using a measurement aperture of 3 mm. Figure 6 shows the measured cross sections through the second patch (dashed line) and fourth patch (solid line) of **Color Plate 12**. From the measurements we see that a luminance variation of 0.022 is present in the second patch and that the variation is increased to 0.04 for the fourth patch. Here, luminance variation was measured

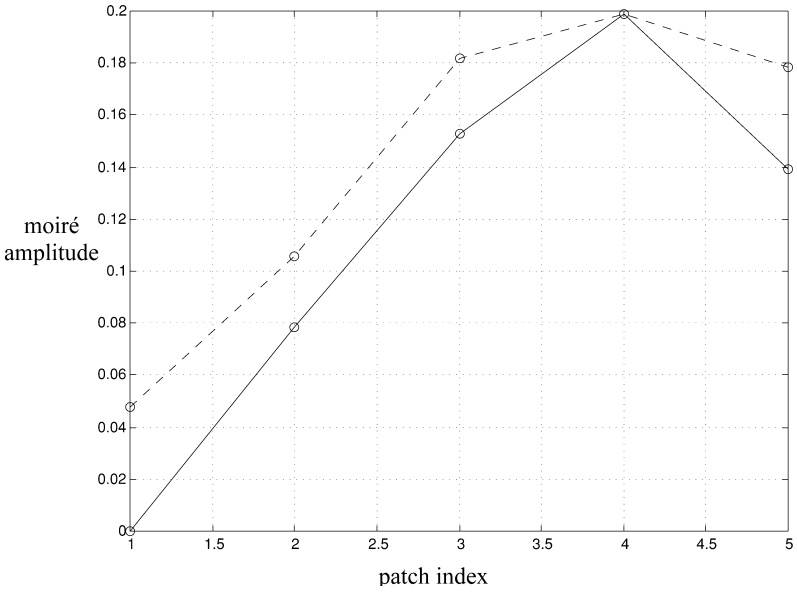

Figure 7. Plot showing measured luminance modulation (dashed) and theoretical moiré amplitude (solid) for the five patches of **Color Plate 12 (p. 173)**. The theoretical values were scaled so that the maxima of the two data sets coincided.

as the difference between the maximum and minimum luminances, averaged over several periods.

A graph comparing the theoretical moiré parameter M and measured luminance variation for the five patches of **Color Plate 12** is shown in Fig. 7. Here the solid line represents the model prediction and the dashed line represents the measurements. The measured data was scaled so that its maximum value coincides with the theoretical maximum. One can see that the model describes the general shape of the moiré dependency on the input *c,m,y,k* quadruplet. The discrepancy between the theoretical amplitude and the actually measured amplitude can be understood by looking at the actual measurements in Fig. 6 and by considering the large fluctuations and consequently large error bars on the measured data.

Experimental Verification of the Modified GCR/UCR Strategy

An experiment verifying the modified UCR/GCR strategy was conducted on a Xerox 5790 laser printer with a resolution of 400 dpi. A clustered rotated dot screen was employed to binarize the contone input. The test image was a three component *c,m,y* sweep from a bluish-purplish color a to a yellowish color, crossing the neutral region. This image was processed through a conventional UCR/GCR strategy with a parabolic black addition function, and *c,m,y* subtraction function that was designed to compensate for the added *k* along the neutral axis. The UCR/GCR algorithm was built into a 3-dimensional lookup table (LUT) from *cmy* to *cmyk* space. The LUT employed a grid of $17 \times 17 \times 17$ nodes. The resulting sweep is shown in the upper part of **Color Plate 13 (p. 173)**. Rendition of this sweep resulted in noticeable moiré through a significant portion of the sweep.

The approach of moiré amplitude restriction was then used to modify the conventional UCR/GCR LUT. Starting with the cmyk quadruplet at a given node of the standard UCR/GCR LUT, a printer model was used to search for a range of alternative c,m,y,k combinations yielding the same printed (i.e. CIELAB) color within a tolerance of $\Delta E^* = 2.0$. The final *cmyk* combination was chosen to be the one closest in Euclidean distance to the original quadruplet corresponding to moiré M less than a predetermined threshold M_{thresh}. This process was repeated for the *cmyk* quadruplets at each of the LUT nodes. The threshold M_{thresh} was chosen to be 0.02, which was the minimum observable moiré amplitude from the visual experiment described previously. The resultant sweep is shown in the lower portion of **Color Plate 13**. No objectionable moiré is visible in this sweep (some moiré might have been introduced by the additional reproduction process for this journal).

The approach of moiré minimization was also tested. This is a slight variant of the moiré amplitude restriction algorithm just described. In this case, for most of the range of the sweep, the search algorithm chooses the 3 colorant (CMY) combinations (since these yield zero moiré). As the sweep approaches black, however, it is not possible to use only C, M, Y to cover the gamut achievable with C, M, Y, K. In these regions, addition of K cannot be avoided. However, fortunately, the visibility of moiré is not high in these regions. The resulting reproduction of the purple-to-yellow sweep is very similar to the bottom image in **Color Plate 13**.

Conclusion

An approach has been described for reducing 3 color moiré in halftone printers by controlling the continuous tone input to the halftoner by means of UCR/GCR adjustment. This approach is based on the observation that

- moiré amplitude is a strong function of area coverages, which are in turn controlled by the UCR/GCR strategy;
- several different *C,M,Y,K* combinations can result in the identical average color with different moiré amplitudes.

A simple and sufficiently accurate model has been derived that relates moiré to input area coverages. The moiré model, in conjunction with a colorimetric printer model, has been used to automatically adjust UCR/GCR

to reduce moiré without sacrificing other factors in color correction such as gamut volume and ink area coverage.

Future work includes the implementation and testing of the other techniques described in this paper, namely the area coverage restriction, and blending algorithms.

Acknowledgment. The authors wish to thank the referees for their valuable comments and suggestions towards improving the quality of this article.

References

1. P. Delabastita, Recent trends in digital halftoning, in *Recent Progress in Digital Halftoning II*, IS&T, Springfield VA, 1999, p. 1.
2. R. W. G. Hunt, *The reproduction of colour*, Fountain Press, London, 1995, p. 612.
3. P. G. Roetling, Halftone method with edge enhancement and moiré suppression, *J. Opt. Soc. Amer.* **66,** 985 (1976).
4. R. Eschbach, A pixel-based error diffusion algorithm producing clustered halftone dots, *J. Electronic Imaging* **3,** 198 (1994).
5. D. N. Knuth, Digital halftones by dot diffusion, *ACM Trans. on Graphics*, **6,** 245 (1987).
6. Z. Fan, Dot-to-dot error diffusion, *J. Electronic Imaging*, **2,** 62 (1993).
7. J. P. Allebach, *Selected Papers On Digital Halftoning*, SPIE Milestone series, 154: Bellingham WA., 1999. (ISBN 0-8194-3137-0).
8. R. Eschbach, *Recent Progress In Digital Halftoning*, IS&T, Springfield VA, 1994 (ISBN 0-89208-181-3).
9. R. Eschbach, *Recent Progress In Digital Halftoning II*, IS&T, Springfield VA, 1999 (ISBN 0-89208-214-3).
10. R. Balasubramanian, R. Eschbach, Design of UCR and GCR strategies to reduce moiré in color printing, *Proc. IS&T PICS*, Savannah, 390 (1999). (ISBN 0-89208-215-1).
11. P. A. Delabastita, Screening techniques, moiré in four color printing, *TAGA*, 44 (1992).
12. C. M. Hains, Method for reducing 2-color moiré in 4-color printing, US Patent 5,381,247 (1995).
13. K. T. Knox, T. Holladay and R. Eschbach, Hybrid halftoning for color moiré reduction, *Proc. SID*, **XXV1,** 837 (1995).
14. R. Balasubramanian, Optimization of the spectral Neugebauer model for printer characterization, *J. Electronic Imaging*, **8,** 156 (1999).